Probing molecular spectral functions and unconventional pairing using Raman spectroscopy

Oriana K. Diessel [1,2,3,4] Jonas von Milczewski [1,2,4,5] Arthur Christianen [1,2] and Richard Schmidt [1,2,5,6]

[1]*Max-Planck-Institute of Quantum Optics, Hans-Kopfermann-Strasse 1, 85748 Garching, Germany*
[2]*Munich Center for Quantum Science and Technology (MCQST), Schellingstrasse 4, 80799 Munich, Germany*
[3]*ITAMP, Center for Astrophysics, Harvard & Smithsonian, Cambridge, Massachusetts 02138, USA*
[4]*Department of Physics, Harvard University, Cambridge, Massachusetts 02138, USA*
[5]*Institute for Theoretical Physics, Heidelberg University, Philosophenweg 16, 69120 Heidelberg, Germany*
[6]*Center for Complex Quantum Systems, Department of Physics and Astronomy, Aarhus University, 8000 Aarhus C, Denmark*

(Received 11 October 2022; accepted 10 April 2024; published 3 June 2024)

An impurity interacting with an ultracold Fermi gas can form either a polaron state or a dressed molecular state, the molaron, in which the impurity forms a bound state with one gas particle. This molaron state features rich physics, including a negative effective mass around unitarity and a first-order transition to the polaron state. However, these features have remained so far experimentally inaccessible. In this work we show theoretically how the molaron state can be directly prepared experimentally even in its excited states using Raman spectroscopy techniques. Initializing the system in the ultrastrong coupling limit, where the binding energy of the molaron is much larger than the Fermi energy, our protocol maps out the momentum-dependent spectral function of the molecule. Using a diagrammatic approach we furthermore show that the molecular spectral function serves as a direct precursor of the elusive Fulde-Ferell-Larkin-Ovchinnikov phase, which is realized for a finite density of fermionic impurity particles. Our results pave the way to a systematic understanding of how composite particles form in quantum many-body environments and provide a basis to develop new schemes for the observation of exotic phases of quantum many-body systems.

DOI: 10.1103/PhysRevResearch.6.023239

I. INTRODUCTION

Understanding the nature of composite particles in a quantum medium is essential to unveil the physics of many intriguing phases of matter. Notable examples include Cooper pairs in superconductors [1,2], the BEC-BCS crossover in ultracold gases [3–11], superfluids of excitons in semiconductors [12,13], anyons such as flux-tube-particle composites [14], and the composite baryons and mesons arising from the quark-gluon plasma in the QCD phase diagram [15].

A paradigmatic system for understanding the formation of such composite particles in a quantum environment is the Fermi polaron problem [16–22]. Here one distinguishable particle (a "quantum impurity") interacts attractively with a bath of indistinguishable fermions. As the attraction between the impurity and the bath increases, a first-order transition is predicted to occur between a polaron state, in which the impurity is dressed by bath fluctuations, and a composite molecule state in which the impurity is bound to one of the bath fermions [23–34]. For even stronger coupling the molecule becomes so tightly bound that it is nearly unaffected by the quantum medium. However, as the transition is approached, the molecule experiences dressing by and exchange with the bath fermions and forms a *molaron* [35], a composite quasiparticle.

Understanding the formation of molarons and their properties in many-body environments is essential to fully describe the general phase diagram of imbalanced Fermi mixtures in ultracold quantum gases and neutron matter [36], as well as the physics of trions in doped, atomically thin semiconductors [37]. However, so far molarons have not been explored experimentally beyond their ground-state properties [38,39]. One of the reasons is that in the impurity limit free-to-bound transitions probe the polaron and not the molaron state due to vanishing overlap with the latter [24]. This hinders the direct creation of composite particles in a Fermi sea and has so far precluded the spectroscopy of molarons including their momentum-resolved excitation spectrum.

In this paper we propose a spectroscopic protocol based on Raman transitions to probe molarons in cold atomic many-body systems. Using this technique allows one to directly measure the momentum-resolved molaron spectral function that encodes all information about the composite quasiparticle including its dispersion, lifetime, effective mass, and full excitation spectrum. Furthermore, using a diagrammatic resummation method, we demonstrate that the finite-momentum properties of the excited molaron state are intimately connected to the emergence of the Fulde-Ferell-Larkin-Ovchinnikov (FFLO) [40,41] phase at finite impurity density, where composite Cooper pairs condense into a finite-momentum state. Our finding highlights a remarkable connection between unconventional superconductivity

and Fermi polarons that allows one to observe fingerprints of complex many-body phases in quantum impurity problems.

II. MICROSCOPIC MODEL

We start by introducing a two-channel Hamiltonian [42] to model the Fermi polaron problem close to a Feshbach resonance:

$$\mathcal{H} = \sum_{\mathbf{p}} \varepsilon^c_{\mathbf{p}} c^\dagger_{\mathbf{p}} c_{\mathbf{p}} + \sum_{\mathbf{p}} \varepsilon^d_{\mathbf{p}} d^\dagger_{\mathbf{p}} d_{\mathbf{p}} + \sum_{\mathbf{p}} (\xi_{\mathbf{p}} + \nu) m^\dagger_{\mathbf{p}} m_{\mathbf{p}} + \frac{h}{\sqrt{V}} \sum_{\mathbf{l},\mathbf{p}} m^\dagger_{\mathbf{p}} c_{\mathbf{l}}\, d_{-\mathbf{l}+\mathbf{p}} + \text{H.c.} \tag{1}$$

Here an impurity ($d^\dagger_{\mathbf{p}}$) interacts with a bath of N fermions ($c^\dagger_{\mathbf{p}}$) in a volume V via the exchange of a bare molecular state in a closed scattering channel ($m^\dagger_{\mathbf{p}}$). The dispersion relations of the impurity and the bath particles are given by $\varepsilon^{d/c}_{\mathbf{p}} = \mathbf{p}^2/2M_{d/c}$, respectively, with momentum $\mathbf{p}$ and masses M_c and $M_d \equiv \alpha M_c$. Here and in what follows, we set $\hbar = 1$. The molecule has a dispersion relation $\xi_{\mathbf{p}} = \mathbf{p}^2/2(1+\alpha)M_c$ and an energy detuning ν which in experiments can be tuned by a magnetic field.

The interaction in the system is described by the last term of Eq. (1), where two fermions in the open scattering channel are converted into the closed-channel molecule. The conversion factor h is proportional to the width of the Feshbach resonance and along with the detuning ν it is tuned to reproduce the s-wave scattering length a and range parameter r^* of the impurity-bath interaction via $\nu_0/h^2 = -\mu/2\pi a + V^{-1}\sum_{\mathbf{k}} 1/(\varepsilon^c_{\mathbf{k}} + \varepsilon^d_{\mathbf{k}})$ [43] and $h^2 = \pi/r^*\mu^2$ with $\mu = M_d M_c/(M_d + M_c)$ [44].

At finite fermion density (determined by the Fermi wave vector $\mathbf{k}_F$ and the corresponding Fermi energy ϵ_F) the impurity is dressed by fluctuations in the Fermi gas and forms a polaron. The molecule in the model is also dressed and forms a composite quasiparticle, the *molaron*. This molaron is adiabatically connected to the molecular bound state at strong coupling. We note that, for light impurities, additional higher-order cluster states may appear in the Fermi polaron problem [45]. These, however, do not play a significant role at the mass ratios considered in this paper. Theoretically both the polaron and molaron can be described using diagrammatic techniques, where the central object is the retarded Green's function:

$$G^R(E, \mathbf{p}) = \mathcal{F}\big[-i\Theta(t)\langle \text{FS}|\big[X^l_{\mathbf{p}}(t), X^\dagger_{\mathbf{p}}(0)\big]_\pm|\text{FS}\rangle\big] \tag{2}$$

with $X_{\mathbf{p}} = d_{\mathbf{p}}(m_{\mathbf{p}})$ for the impurity (molecule) and $[\cdot,\cdot]_\pm$ the (anti)commutator. Here $\mathcal{F}$ denotes the Fourier transform from time t to frequency space E. The poles of $G^R(E, \mathbf{p})$ directly yield the energy of the attractive and repulsive polaron (molaron) as schematically shown in Fig. 1. As can be seen in the figure, the molaron also exists as an excited state in the interaction regime where the attractive polaron is the ground state. Remarkably, the molaron is stabilized even in the regime of negative scattering lengths where in the model (1) no molecule exists in vacuum, reminiscent of Cooper pairing in the theory of superconductivity [1,2].

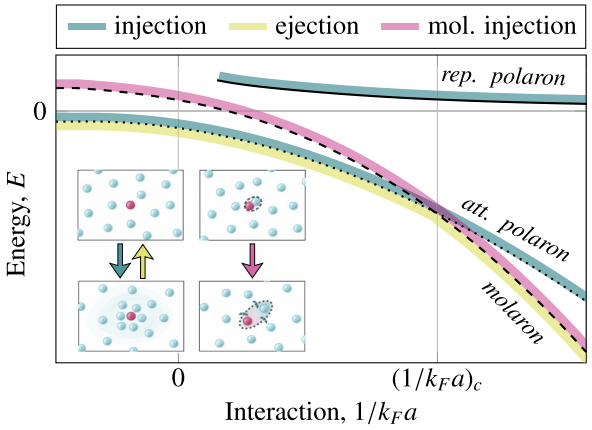

FIG. 1. Schematic figure of the polaron (dotted black line) to molaron (dashed black line) transition in a mass-balanced system close to a broad Feshbach resonance. The inset displays the different spectroscopic schemes in ultracold quantum gases: In injection spectroscopy (blue arrow), an initially noninteracting impurity is injected into a state in which it can interact with the bath particles. This technique allows for the detection of the polaron, but suffers from a vanishing overlap between the noninteracting ground state and the molaron state. In ejection spectroscopy (yellow arrow), the interacting impurity gets ejected into a noninteracting state, which allows for the detection of the ground state (yellow). Our proposal (pink arrow) enables the detection of the excited molaron branch, by initializing the system in the ultrastrong coupling limit.

The single-particle spectral function can be obtained via $\mathcal{A}(E, \mathbf{p}) = \text{Im}\, G^R(E, \mathbf{p})$ and is shown for the molecule at unitarity, $a \to \infty$, in the leftmost plot of Fig. 2(a), obtained using a non-self-consistent T-matrix resummation approach. The molaron can be seen as a sharp peak in the spectral function. At a finite momentum $\mathbf{k}$, it intersects the continuum of incoherent particle-hole excitations delimited by a parabola of the form $(|\mathbf{k}| - k_F)^2$. The molaron dispersion shows a minimum at finite momentum [31,33,39,45,46] (see Refs. [47,48] for the two-dimensional case), a finding robust with respect to the theoretical approximation scheme.

III. PRECURSOR OF THE FFLO PHASE

We now directly connect the existence of the molaron dispersion minimum at finite momentum to the emergence of the elusive FFLO phase of superconductivity [49,50]. Extending the T-matrix approach to finite *fermionic* impurity density, at fixed bath chemical potential $\mu_c = \epsilon_F$ we keep track of the *bosonic* molaron spectral function in dependence on the impurity chemical potential μ_d. As can be seen in Fig. 2(a), with increasing impurity chemical potential μ_d the dispersion minimum continuously evolves until the finite-momentum molaron becomes gapless precisely at the predicted onset of the FFLO phase at $\mu_d = 0.196\,\epsilon_F$ [51]. This continuous relation of the molaron spectral function towards a gapless spectrum implies a simple picture of the FFLO phase as a condensate of molarons.

To further substantiate this direct connection between molarons and the formation of the FFLO phase, we investigate

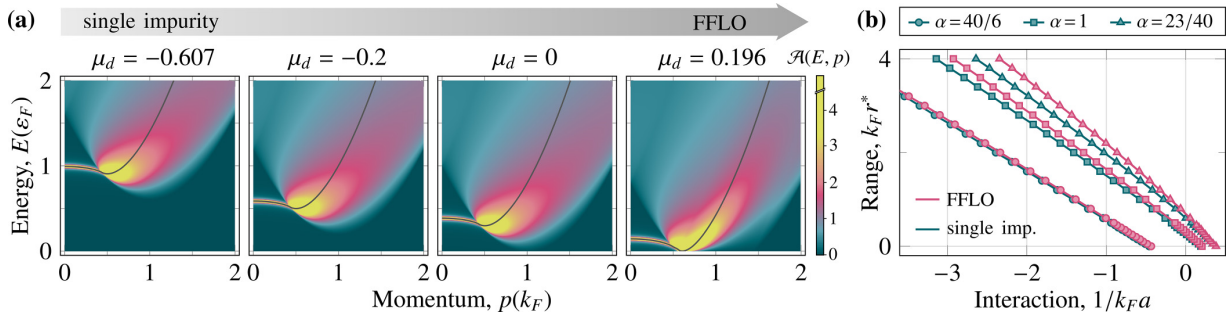

FIG. 2. (a) Density plot of the molaron spectral function $\mathcal{A}(E, \mathbf{p})$ in units of ε_F at unitarity in the contact interaction limit ($k_F r^* = 0$) and mass balance ($\alpha = 1$) for different chemical potentials of the minority population. The molaron dispersion (gray line) has a minimum at finite momentum. For $\mu_d = 0.196\,\epsilon_F$, the molaron becomes gapless at finite momentum, which determines the onset of the FFLO phase. (b) Critical range parameter $k_F r^*$ below which the molaron dispersion minimum is at finite momentum (blue) and for which the FFLO phase occurs at finite impurity density (pink), shown for the mass ratios $\alpha = 40/6$ (heavy impurity), $\alpha = 1$ (mass balance), and the hypothetical mass ratio $\alpha = 23/40$ (light impurity) as a function of the interaction strength.

its dependence on interaction strengths and the range parameter. The transition towards the FFLO phase can be found by solving the Cooper problem at finite momentum $|\mathbf{p}| > 0$ [51]. Here, we extend this approach to the two-channel model (1) which accounts also for a finite effective range parameter r^*. To this end, we determine the poles of the molecule's Green's function (2) where $X_\mathbf{p} = m_\mathbf{p}$, which can be found by solving for

$$-E + \xi_\mathbf{p} - \mu_d - \mu_c + \frac{\pi}{r^*\mu^2}\left[\frac{\mu}{2\pi a} - \frac{1}{V}\sum_\mathbf{k} \times \left(\frac{1}{\varepsilon^c_\mathbf{k} + \varepsilon^d_\mathbf{k}} - \frac{1 - n_F(\varepsilon^c_\mathbf{k}, \mu_c) - n_F(\varepsilon^d_{-\mathbf{k}+\mathbf{p}}, \mu_d)}{-E - i0^+ + \varepsilon^c_\mathbf{k} - \mu_c + \varepsilon^d_{-\mathbf{k}+\mathbf{p}} - \mu_d}\right)\right] = 0, \tag{3}$$

with $n_F(\varepsilon, \tilde{\mu}) = (e^{\frac{1}{T}(\varepsilon - \tilde{\mu})} + 1)^{-1}$ the Fermi-Dirac distribution function at chemical potential $\tilde{\mu}$. The inverse molecular Green's function shown in Eq. (3) features a self-energy renormalization containing an impurity-bath particle-particle bubble, which for vanishing range parameter r^* is closely related to a non-self-consistent T-matrix approximation.

We now explore the possibility of the appearance of an FFLO phase as a function of the interaction strength and effective range. Starting from an impurity vacuum at sufficiently negative impurity chemical potential μ_d, we increase μ_d until the lowest-lying solution of Eq. (3) is found at $E = 0$. If this solution is found at finite $|\mathbf{p}| > 0$, an FFLO phase is formed. For different mass ratios down to $\alpha \approx 0.6$, the boundary of the FFLO phase is shown in Fig. 2(b) as pink lines. The trimer states and higher order clusters which can form for light impurities [45] do not yet play a role in this parameter regime.

We now compare the predicted critical value of the FFLO transition to the critical interaction strengths at which the minimum of the molaron dispersion moves to finite momentum [see Fig. 2(b) blue lines]. As can be seen, the boundaries lie in close proximity and exhibit the same behavior with respect to the tuning of the range parameter r^*. Based on this close correspondence, we conclude that the transition point towards the FFLO phase can already be inferred from the excited composite states in the Fermi polaron problem.

In Fig. 2(b), the onset of the finite-momentum minimum in the molecule spectral function in the single impurity limit, and likewise the transition towards the FFLO phase at a finite density imbalance, appear at smaller interaction strengths as the range parameter r^* increases. The effect of r^* was studied in some detail in Ref. [52] in the context of static impurities immersed in a Fermi gas. Based on these results we conjecture that the general trend can be explained by the effectively larger scattering phase shift at the Fermi surface as r^* is increased. We leave a more in-depth study of this interesting effect to future research.

Finally, we note that in finite-density mixtures the formation of FFLO order is sometimes prevented by phase separation [49,53–55], which is not included in our calculations. In fact it was shown [51] that the FFLO state is the true ground state of the system only in a small region of parameter space, which makes it difficult to detect. However, in the impurity limit, phase separation does not exist by construction. The direct connection between molarons and the formation of the FFLO phase therefore gives an exciting opportunity to witness a precursor of the FFLO phase already in a much broader and more easily reachable parameter regime.

IV. MOLECULAR INJECTION SPECTROSCOPY

Despite its importance for emerging many-body phases, the molaron has not been observed in experiments at interaction strengths below the transition (see Fig. 1) [34,37–39,56]. Here we propose a generalization of atomic Raman spectroscopy to allow for observing composite states including their full excitation spectrum. In Raman spectroscopy lasers induce transfers between internal atomic degrees of freedom adding a momentum $\mathbf{q}_L$ and an energy ω to the atoms [39,57–59].

Within linear response theory the absorption rate with respect to the perturbing atomic transition operator $\hat{V}_{\mathbf{q}_L}$ is given

by Fermi's golden rule,

$$\mathcal{R}(\omega, \mathbf{q}_L) = \sum_{\alpha} \left|\langle\alpha|\hat{V}_{\mathbf{q}_L}|i\rangle\right|^2 \delta(\omega - E_\alpha + E_i), \tag{4}$$

where $|i\rangle$, $\{|\alpha\rangle\}$ and E_i, E_α denote the initial state and a basis set of final states and their respective energies. The polaron spectral function can be measured by choosing an initial state in which the impurity and the Fermi gas do not interact with each other. The transition operator then transfers the impurity to a final state in which it interacts with the fermions. In such injection spectroscopy the Raman response is identical to the polaron spectral function (see Ref. [34] for rf spectroscopy, $\mathbf{q}_L = 0$, which has been successfully employed to observe Fermi polarons). The reason that injection spectroscopy is not suitable to study molaron states is the difference in the structure of the background Fermi sea for polarons and molarons. It requires multiple quasiparticle excitations to go from the polaron to the molaron state [24], making these processes strongly suppressed when the energy gap between the polaron and molaron goes to zero (in injection spectra only the polaron is visible as a sharp feature and the observed molecule-hole continuum stems from a superposition of many molarons at all different momenta [34]). This is in contrast to mixtures with finite impurity density or thermal gases. In this case, the same argument does not apply, and free-to-bound transitions, in fact, are an important tool to create and characterize Feshbach molecules [60–64].

In ejection spectroscopy, on the other hand, an initially interacting impurity gets ejected into a noninteracting state. This technique allows only for the detection of the ground state. Moreover, finite-momentum properties of the molaron are not accessible.

We now show how the idea of injection spectroscopy can be extended to make the full excitation spectrum of molarons accessible. The idea can most easily be theoretically explained using a wave function picture. To this end it is helpful to realize that the diagrammatic calculation leading to G^R_{mol} in Fig. 2(a) is equivalent to diagonalizing the problem in a truncated Hilbert space corresponding to a molaron wave function ansatz [26,27,33]:

$$|M^{\mathbf{p}}\rangle = \alpha^{\mathbf{p}} m^\dagger_{\mathbf{p}}|\text{FS}_{N-1}\rangle + \sum_{\mathbf{k}} \beta^{\mathbf{p}}_{\mathbf{k}} c^\dagger_{-\mathbf{k}} d^\dagger_{\mathbf{k}+\mathbf{p}}|\text{FS}_{N-1}\rangle. \tag{5}$$

This ansatz is an extension of the vacuum solution and creates a molecule on top of a Fermi sea $|\text{FS}_{N-1}\rangle$ with $N-1$ atoms. The vanishing overlap in injection spectroscopy highlights how the choice of an initial state is the key to measuring molecular properties. The state should fulfill two main criteria:

(a) It has to be a good reference state, i.e., a state that can be reliably prepared and whose properties are well understood.

(b) It should have sufficient spectroscopic overlap with the final state of interest, in this case the molecular state in the quantum medium.

We now show that starting from a relatively deeply bound molecular state one can fulfill both criteria, which allows one to reliably probe many-body dressed composites in what we term *molecular injection spectroscopy*. In density-balanced systems, similar bound-to-bound transitions have been employed to determine the zero momentum energy of the bound states in the final state [66].

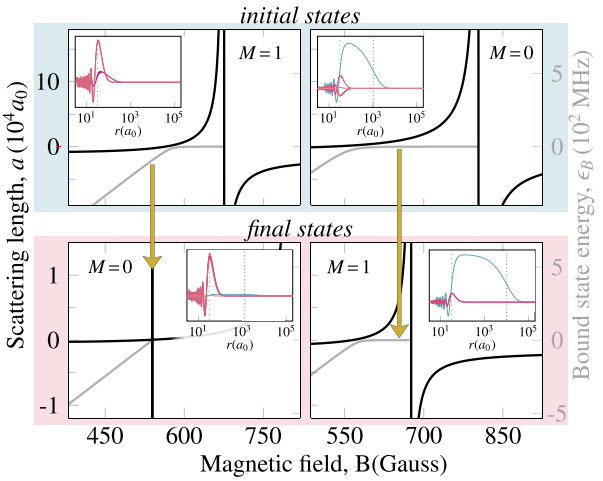

FIG. 3. Experimental protocol for the example of ^{6}Li. Scattering length (solid black) as a function of magnetic field for the initial state (top, blue) and final state (bottom, red). In the left (right) panels one aims to probe a molaron in a final state at a narrow (broad) Feshbach resonance. The insets show the different channel contributions to the radial wave function of the Feshbach molecule at the applied magnetic field: open channels (blue) and closed channels (pink). In the top right plot the narrow resonance is omitted for clarity. All data are obtained from a coupled-channel calculation, using realistic atomic potentials as input [65]. Dashed (dotted) lines in the insets indicate the van der Waals and scattering lengths, respectively.

In this scheme, the first criterion is fulfilled by starting from a molecular state with binding energy $\epsilon_{B,\text{in}}/\epsilon_F \gg 1$ so that medium corrections determined by the Fermi energy ϵ_F are negligible. As a result, the initial state is well described by typical atomic physics models [44]. Establishing the fulfillment of the second condition requires a detailed analysis of the action of the Raman operator $\hat{V}_{\mathbf{q}_L}$ on this initial state.

Within our two-channel model, understanding the action of the Raman lasers requires translation of $\hat{V}_{\mathbf{q}_L}$ from an atomic state basis (where it takes a form $\sim \sum_{\mathbf{p}} d^\dagger_{\mathbf{p}+\mathbf{q}_L,f} d_{\mathbf{p},i}$, with i, f labeling the internal atomic states of the impurity before and after the Raman transition) into a basis that explicitly accounts for the closed-channel molecule $m^\dagger$ that arises from having integrated out atom fluctuations in the closed channel. To achieve this we turn to an *ab initio* coupled-channel calculation in the two-body limit. Considering here the two-body limit is justified since the initial state is tightly bound and many-body dressing of the final state molecule only affects its low energy physics, and hence does not affect the form of the laser operator.

The *ab initio* calculation is described in the Appendix A. It is based on atomic states and yields not only the binding energies and the magnetic field dependent scattering lengths, but also allows for a clear distinction between the open-channel (long-range component) and closed-channel (short-range component) contributions to the molecular wave functions [67]; see Fig 3. For concreteness we consider

here exclusively the example of ^{6}Li, which features all key elements to demonstrate the idea of molecular injection spectroscopy. Specifically, we focus on two limits where the initial state molecule has either its weight almost entirely in the closed channels (cf. Fig. 3, upper left), or in the open channel (upper right), allowing for a precise characterization of the Raman laser operator.

The left-hand panels in Fig. 3 show the scenario of a strongly bound closed-channel Feshbach molecule in the initial state, corresponding to $|i\rangle = m^\dagger_{\mathbf{0},i}|0\rangle$ in our model. Such a state can be prepared for sufficient detuning from a Feshbach resonance, possible for both narrow and broad resonances. This choice of initial state (the wave functions including their hyperfine state contributions are shown as insets in Fig. 3; see Appendix A) is ideal to detect molarons in the final state close to a narrow resonance, due to a large spectroscopic overlap between initial and final closed-channel contributions (compare insets in Fig. 3). Furthermore, with a size on the order of the van der Waals length l_{vdW} (dashed, vertical lines in insets), the initial closed-channel contributions yield only small overlap with the spatially extended open-channel states in the final state. As a consequence, the Raman operator is well approximated as $\hat{V}_{\mathbf{q}_L} = \sum_{\mathbf{p}} m^\dagger_{\mathbf{p}+\mathbf{q}_L,f} m_{\mathbf{p},i}$ in the two-channel model.

A second option, best suited to detect molarons close to a broad resonance in the final state, is to start from a deeply bound initial molecular state close to an open-channel dominated resonance (see right-hand panels in Fig. 3). Note that, compared to the previous scenario, the initial state is less deeply bound and is in the regime where its energy does not depend linearly on the B field. As the coupled-channel calculation shows, the initial state is dominated by open-channel contributions. In the two-channel model this state is described by $|i\rangle = \sum_{\mathbf{k}} \beta^{\mathbf{0}}_{\mathbf{k}} c^\dagger_{-\mathbf{k}} d^\dagger_{\mathbf{k},i}|0\rangle$. Thus the Raman laser mostly acts on that contribution which is confined on the order of the scattering length a (dotted vertical line in the inset of Fig. 3), and transferred to open-channel contributions in the final state manifold. The projection onto closed channels of the final state manifold has a negligible contribution due to lacking overlap of these states at low energy. Hence, within the two-channel model the Raman operator is well represented by $\hat{V}_{\mathbf{q}_L} = \sum_{\mathbf{p}} d^\dagger_{\mathbf{p}+\mathbf{q}_L,f} d_{\mathbf{p},i}$.

V. THEORETICAL RAMAN SPECTRA

Having established the form of the operator $\hat{V}_{\mathbf{q}_L}$ we now turn to the prediction of the Raman absorption $\mathcal{R}(\omega, \mathbf{q}_L)$. To this end, using the identity $\lim_{y\to 0^+} 1/(x+iy) = -i\pi\delta(x) + \mathcal{P}(1/x)$ and replacing $E_\alpha|\alpha\rangle = \mathcal{H}|\alpha\rangle$, we eliminate the explicit final state dependence in Eq. (4):

$$\mathcal{R}(\omega, \mathbf{q}_L) = -\frac{1}{\pi}\,\mathrm{Im}\langle i|\hat{V}^\dagger_{\mathbf{q}_L}\frac{1}{\omega - \mathcal{H} + E_i + i0^+}\hat{V}_{\mathbf{q}_L}|i\rangle. \quad (6)$$

Here, the initial state $|i\rangle$ is given by a molecule state of form (5) with energy $\epsilon_{B,in} \gg \epsilon_F$ such that the many-body dressing by bath particles is negligible.

Using a basis truncation that includes up to one excitation on top of the Fermi sea, the Raman response takes the form

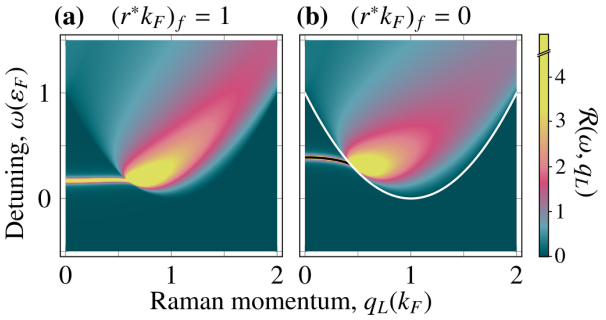

FIG. 4. Raman spectra at unitarity and mass balance. (a) Narrow Feshbach resonance ($r^*k_F = 1$) in the final state. The Raman spectrum equals the molaron spectral function. (b) Broad Feshbach resonance ($r^*k_F = 0$) in the final state and initial state at $1/ak_F = 1.5$. The Raman spectrum reproduces all key spectral features such as the onset of the continuum (white line) and sharp quasiparticle excitations (black line). Initial state energies are subtracted in both spectra.

(for details see Appendix)

$$\mathcal{R}(\omega, \mathbf{q}_L) = -\frac{1}{\pi}\,\mathrm{Im}\left(f^{\mathbf{q}_L}(\omega) G^R_{\mathrm{mol}}(\mathbf{q}_L, \omega)\right) + \sum_{\mathbf{k}} |\tilde{\beta}^{\mathbf{q}_L}_{\mathbf{k}}|^2 \times \delta\left(\omega + E_{\mathrm{mol},i} - E_{\mathrm{FS}_{N-1}} - \varepsilon^c_{\mathbf{k}} - \varepsilon^d_{\mathbf{q}_L+\mathbf{k}}\right), \quad (7)$$

where $\tilde{\beta}^{\mathbf{q}_L}_{\mathbf{k}}$ is the open-channel contribution of $\hat{V}_{\mathbf{q}_L}|i\rangle$ and $f^{\mathbf{q}_L}$ is a multiplicative structure factor. Equation (7) shows the direct connection between the Raman response and the molaron Green's function G^R_{mol}. Exemplary spectra are shown in Fig. 4.

In the case of a narrow Feshbach resonance in the final state [Fig. 4(a)], we choose a deeply bound initial state given by $|i\rangle = m^\dagger_{i,\mathbf{0}}|\mathrm{FS}_{N-1}\rangle$. In this case, $\tilde{\beta}^{\mathbf{q}_L}_{\mathbf{k}} = 0$ and $f^{\mathbf{q}_L} \equiv 1$, such that the Raman spectrum and the molecular spectral function exactly coincide, $\mathcal{R} = \mathcal{A}_{\mathrm{mol}}$.

Next we turn to a broad Feshbach resonance in the final state ($|i\rangle = \sum_{\mathbf{k}} \beta^{\mathbf{0}}_{\mathbf{k}} c^\dagger_{-\mathbf{k}} d^\dagger_{\mathbf{k},i}|\mathrm{FS}_{N-1}\rangle$). In Fig. 4(b) it can be seen that the Raman spectrum contains the same qualitative features as the corresponding molaron spectral function shown in Fig. 2(a); in particular the position of the molaron as well as its merging into the continuum can be inferred from the Raman spectrum. Quantitatively, the difference between these spectra is merely a redistribution of spectral weight where the second part of Eq. (7) has negligible contribution [68]. Importantly, the dispersion relation of the molaron including its finite momentum minimum is contained in such Raman spectra. Therefore, our approach allows one to observe a key signature of the instability towards the FFLO phase both for broad and narrow Feshbach resonances.

VI. CONCLUSION

In this work we have presented a protocol to measure the momentum-resolved molaron spectral function at arbitrary interaction strengths. This is achieved using Raman injection spectroscopy with a tunable transfer momentum, where the system is initialized in the ultrastrong coupling limit. In combination with standard injection spectroscopy, which allows

for the detection of the polaron branch, this would allow for the simultaneous observation of both polaron and molaron branches at the same interaction strength, which provides an experimental tool to prove not only their coexistence but also the first-order nature of their transition [69–71]. Our results show the robustness of this approach to observe the nontrivial dispersion relations of composite states, including the formation of a roton-type minimum. Furthermore, we demonstrated that this finite-momentum minimum in the molaron spectral function is a precursor of the elusive FFLO phase.

Our approach can be equally applied to the case of Bose polarons, where the resulting composite is fermionic. Such impurity systems hold promise to exhibit precursors of topologically non-trivial Fermi surfaces and Fermi surface reconstruction. Furthermore, it may allow to shed new light on the role of many-body bound states involving more than one bath atom as well as emerging phases in mass-imbalanced ultracold gases [72].

ACKNOWLEDGMENTS

We thank Yoav Sagi, Gal Ness, and Selim Jochim for inspiring discussions. We acknowledge support by the Deutsche Forschungsgemeinschaft under Germany's Excellence Strategy xEXC-2111-390814868 and EXC 2181/1-390900948 (the Heidelberg STRUCTURES Excellence Cluster) and the Collaborative Research Centre SFB 1225 (ISOQUANT). This work was supported by the Danish National Research Foundation through the Center of Excellence "CCQ" (Grant No.DNRF156). O.K.D. and J.v.M. are supported by fellowships of the International Max Planck Research School for Quantum Science and Technology (IMPRS-QST).

APPENDIX A: COUPLED-CHANNEL CALCULATION FOR TWO-BODY PROBLEM

In this Appendix we provide supplementary information on the coupled-channel calculation leading to the results presented in the main text (see for example Ref. [65]). The aim is to find the scattering lengths, bound-state energies and wave functions for two interacting ^{6}Li atoms, labeled by indices 1 and 2, in an external magnetic field B. Neglecting magnetic dipole interactions and assuming zero rotational angular momentum (s-wave scattering), the Hamiltonian in the center of mass frame of this system is given by

$$\hat{\mathcal{H}} = \hat{\mathcal{H}}_{\mathrm{Li}}(\hat{\mathbf{I}}_1, \hat{\mathbf{S}}_1, B) + \hat{\mathcal{H}}_{\mathrm{Li}}(\hat{\mathbf{I}}_2, \hat{\mathbf{S}}_2, B) - \frac{1}{2\mu R}\frac{\partial^2}{\partial R^2}R + V(R, \hat{\mathbf{S}}_1, \hat{\mathbf{S}}_2). \tag{A1}$$

Here $\hat{\mathbf{I}}_i$, $\hat{\mathbf{S}}_i$ denote the nuclear and electronic spin operators of the two particles, R is the interatomic distance, μ the reduced mass, V the interaction potential, and $\hat{\mathcal{H}}_{\mathrm{Li}}$ the Hamiltonian of a free lithium atom in a magnetic field [73]. We use singlet and triplet interaction potentials [65] which have been optimized to match experiments.

We can now express the wave function in terms of the asymptotic spin eigenbasis, denoted by $|i\rangle$, and a position basis in R:

$$|\Psi(R)\rangle = \hat{P}_{\mathrm{asym}}\frac{1}{R}\sum_i \psi_i(R)|i\rangle. \tag{A2}$$

We have included a geometric factor R in the definition of the radial wave function contribution ψ_i to channel i, and $\hat{P}_{\mathrm{asym}}$ is the antisymmetrization operator.

In terms of the variables ψ_i, the problem now reduces to a second-order matrix-valued differential equation in R, which we solve with the renormalized Numerov method [74] with variable step size [75]. Since the total projection $M = \hat{\mathbf{I}}_1^z + \hat{\mathbf{S}}_1^z + \hat{\mathbf{I}}_2^z + \hat{\mathbf{S}}_2^z$ of the angular momentum on the magnetic field axis is conserved, the scattering or bound-state problem can be solved separately for every value of M. For every M different combinations of the electronic and nuclear spins can contribute. An example of a channel in the $M = 0$ manifold is $|m_{s_1} = 1/2,\ m_{I_1} = 1,\ m_{s_2} = -1/2,\ m_{I_2} = -1\rangle$. For ultracold collisions of ground-state atoms, one channel asymptotically lies below the scattering threshold ("open") and several lie above ("closed").

The radial wave functions are shown in Fig. 3 for the $M = 1$ and $M = 0$ scattering manifolds of ^{6}Li for given magnetic field strengths. Here we have drawn the open channel in blue and the closed channels in pink. One can then compute the corresponding bound state energies, which are shown as grey lines in the main panels of Fig. 3. From the long-distance properties of scattering wave functions one can furthermore extract the corresponding scattering lengths, shown as black lines in Fig. 3.

APPENDIX B: COMPUTATION OF RAMAN SPECTRA

In order to compute the Raman spectra defined in Eq. (6) of the main text, the matrix elements of the resolvant operator $(\rho - \mathcal{H})^{-1}$ need to be determined on the final state manifold spanned by states of the form $m^\dagger_{\mathbf{q}_L,f}|\mathrm{FS}_{N-1}\rangle$ and $\{c^\dagger_{-\mathbf{k}}d^\dagger_{\mathbf{k}+\mathbf{q}_L,f}|\mathrm{FS}_{N-1}\rangle\}$ with $\rho = \omega + E_i + i0^+$ and $|\mathbf{k}| > k_F$. To this end, we rewrite the operator as

$$\frac{1}{\rho - \mathcal{H}} = \frac{1}{\rho - \epsilon} + \frac{1}{\rho - \mathcal{H}}\,T\,\frac{1}{\rho - \epsilon}, \tag{B1}$$

where ϵ and T denote the kinetic and interaction terms of the Hamiltonian in Eq. (1), respectively. Defining

$$|0\rangle = m^\dagger_{\mathbf{q}_L,f}|\mathrm{FS}_{N-1}\rangle, \tag{B2}$$

$$|\mathbf{k}\rangle = c^\dagger_{-\mathbf{k}}d^\dagger_{\mathbf{k}+\mathbf{q}_L,f}|\mathrm{FS}_{N-1}\rangle \tag{B3}$$

along with

$$\epsilon^0 = \xi_{\mathbf{q}_L} + \nu + E_{\mathrm{FS}}(N-1), \tag{B4}$$

$$\epsilon_{\mathbf{k}} = \varepsilon^c_{\mathbf{k}} + \varepsilon^d_{\mathbf{q}_L+\mathbf{k}} + E_{\mathrm{FS}}(N-1), \tag{B5}$$

one arrives at the following system of equations:

$$\langle 0|\frac{1}{\rho - \mathcal{H}}|0\rangle = \frac{1}{\rho - \epsilon^0} + \frac{1}{\rho - \epsilon^0}\langle 0|\frac{1}{\rho - \mathcal{H}}\frac{h}{\sqrt{V}}\sum_{\mathbf{k}},$$

$$\langle 0|\frac{1}{\rho - \mathcal{H}}|\mathbf{k}\rangle = \frac{1}{\rho - \epsilon_{\mathbf{k}}}\langle 0|\frac{1}{\rho - \mathcal{H}}\frac{h}{\sqrt{V}}|0\rangle,$$

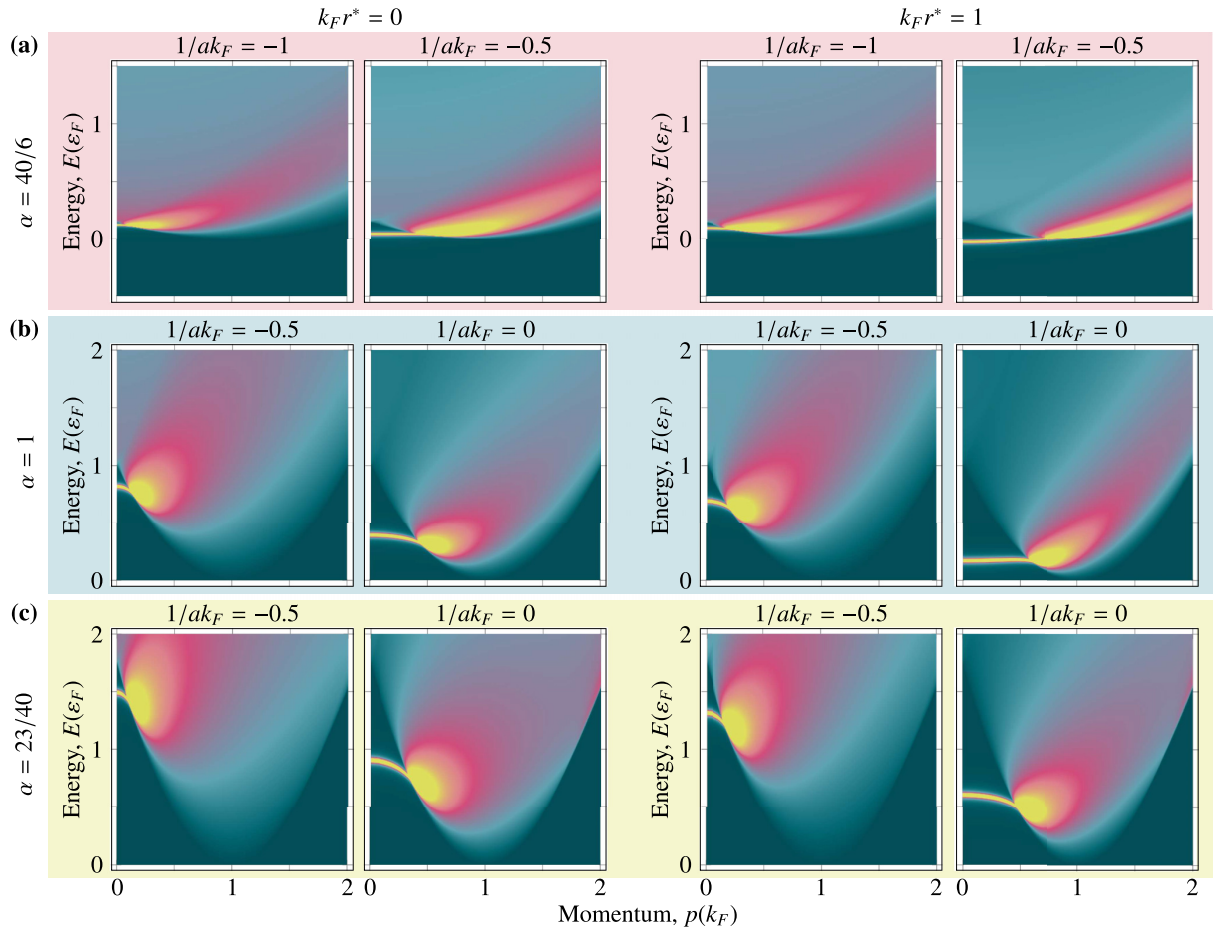

FIG. 5. Molaron spectral function for different ranges $k_F r^*$, interactions $1/ak_F$, and mass imbalances α.

$$\langle \mathbf{k}|\frac{1}{\rho-\mathcal{H}}|0\rangle = \frac{1}{\rho-\epsilon^0}\langle \mathbf{k}|\frac{1}{\rho-\mathcal{H}}\frac{h}{\sqrt{V}}\sum_{\mathbf{k}'}|\mathbf{k}'\rangle,$$
$$\langle \mathbf{k}'|\frac{1}{\rho-\mathcal{H}}|\mathbf{k}\rangle = \frac{\delta_{\mathbf{k},\mathbf{k}'}}{\rho-\epsilon_{\mathbf{k}}} + \frac{1}{\rho-\epsilon_{\mathbf{k}}}\langle \mathbf{k}'|\frac{1}{\rho-\mathcal{H}}\frac{h}{\sqrt{V}}|0\rangle. \tag{B6}$$

Here, we only kept terms up to a single particle-hole excitation (similar to the non-self-consistent T-matrix approximation), which allows one to solve the system of equations

$$\langle 0|\frac{1}{\rho-\mathcal{H}}|0\rangle = \frac{1}{h^2}\frac{1}{\frac{\rho-\epsilon^0}{h^2} - \frac{1}{V}\sum_{\mathbf{k}''}\frac{1}{\rho-\epsilon_{\mathbf{k}''}}},$$
$$\langle 0|\frac{1}{\rho-\mathcal{H}}|\mathbf{k}\rangle = \frac{1}{\sqrt{V}h}\frac{1}{\rho-\epsilon_{\mathbf{k}}}\frac{1}{\frac{\rho-\epsilon^0}{h^2} - \frac{1}{V}\sum_{\mathbf{k}''}\frac{1}{\rho-\epsilon_{\mathbf{k}''}}},$$
$$\langle \mathbf{k}'|\frac{1}{\rho-\mathcal{H}}|0\rangle = \frac{1}{\sqrt{V}h}\frac{1}{\rho-\epsilon_{\mathbf{k}'}}\frac{1}{\frac{\rho-\epsilon^0}{h^2} - \frac{1}{V}\sum_{\mathbf{k}''}\frac{1}{\rho-\epsilon_{\mathbf{k}''}}},$$

$$\langle \mathbf{k}'|\frac{1}{\rho-\mathcal{H}}|\mathbf{k}\rangle = \frac{\delta_{\mathbf{k},\mathbf{k}'}}{\rho-\epsilon_{\mathbf{k}}} + \frac{1}{V}\frac{1}{\rho-\epsilon_{\mathbf{k}}}\frac{1}{\rho-\epsilon_{\mathbf{k}'}} \times \frac{1}{\frac{\rho-\epsilon^0}{h^2} - \frac{1}{V}\sum_{\mathbf{k}''}\frac{1}{\rho-\epsilon_{\mathbf{k}''}}}, \tag{B7}$$

where all sums are restricted to $|\mathbf{k}''| > k_F$. As can be seen, the retarded molecular Green's function given by

$$G^R(\omega, \mathbf{q}_L) = \langle 0|(\rho-\mathcal{H})^{-1}|0\rangle \tag{B8}$$

reappears within all other matrix elements of $(\rho-\mathcal{H})^{-1}$. For two arbitrary overlapping Feshbach resonances, after acting with the Raman lasers on an initial state given by Eq. (5) in the main text, the resulting state is given by

$$V_L^{\mathbf{q}_L}|i\rangle = \tilde{\beta}_0^{\mathbf{q}_L} m^\dagger_{\mathbf{q}_L,f}|\mathrm{FS}_{N-1}\rangle + \sum_{\mathbf{k}}\tilde{\beta}_{\mathbf{k}}^{\mathbf{q}_L} c^\dagger_{-\mathbf{k}} d^\dagger_{\mathbf{k}+\mathbf{q}_L,f}|\mathrm{FS}_{N-1}\rangle. \tag{B9}$$

Here the relative weights between the closed and open channel contributions $\tilde{\beta}_0^{\mathbf{q}_L}$, $\tilde{\beta}_{\mathbf{k}}^{\mathbf{q}_L}$ can in general be different from the

ones in Eq. (5), as they depend on the form of the Raman laser operator.

Finally, given knowledge of the $\tilde{\beta}_0^{\mathbf{q}_L}, \tilde{\beta}_{\mathbf{k}}^{\mathbf{q}_L}$, the Raman response function of two arbitrary overlapping Feshbach resonances is given by

$$\mathcal{R}^{\mathbf{q}_L}(\omega) = -\frac{1}{\pi}\,\mathrm{Im}\left(\left|\tilde{\beta}_0^{\mathbf{q}_L}\right|^2\langle 0|\frac{1}{\rho-\mathcal{H}}|0\rangle + \sum_{\mathbf{k}} 2\,\mathrm{Re}\left[\tilde{\beta}_{\mathbf{k}}^{\mathbf{q}_L *}\tilde{\beta}_0^{\mathbf{q}_L}\right]\langle \mathbf{k}|\frac{1}{\rho-\mathcal{H}}|0\rangle + \sum_{\mathbf{k}\mathbf{k}'}\tilde{\beta}_{\mathbf{k}'}^{\bar{\mathbf{q}}*}\tilde{\beta}_{\mathbf{k}}^{\mathbf{q}_L}\,\langle \mathbf{k}'|\frac{1}{\rho-\mathcal{H}}|\mathbf{k}\rangle\right). \tag{B10}$$

Thus, it can easily be seen that with the exception of the (trivial) first term within $\langle \mathbf{k}'|\frac{1}{\rho-H}|\mathbf{k}\rangle$ the resulting Raman response function contains the molecular Green's function, i.e.,

$$\mathcal{R}^{\mathbf{q}_L}(\omega) = -\frac{1}{\pi}\,\mathrm{Im}(f^{\mathbf{q}_L}(\omega)G^R(\mathbf{q}_L,\omega)) + \sum_{\mathbf{k}}|\tilde{\beta}_{\mathbf{k}}^{\mathbf{q}_L}|^2\delta(\mathrm{Re}(\rho)-\epsilon_{\mathbf{k}}), \tag{B11}$$

where the proportionality function is given by

$$f^{\mathbf{q}_L}(\omega) = \left|\tilde{\beta}_0^{\mathbf{q}_L}\right|^2 + \sum_{\mathbf{k}} 2\,\mathrm{Re}\left[\tilde{\beta}_{\mathbf{k}}^{\mathbf{q}_L *}\tilde{\beta}_0^{\mathbf{q}_L}\right]\frac{h}{\sqrt{V}}\frac{1}{\rho-\epsilon_{\mathbf{k}}} + \sum_{\mathbf{k}\mathbf{k}'}\tilde{\beta}_{\mathbf{k}'}^{\bar{\mathbf{q}}*}\tilde{\beta}_{\mathbf{k}}^{\mathbf{q}_L}\frac{h^2}{V}\frac{1}{\rho-\epsilon_{\mathbf{k}}}\frac{1}{\rho-\epsilon_{\mathbf{k}'}}. \tag{B12}$$

In the main text, we discuss in detail the two scenarios of a narrow and a broad Feshbach resonance in the final state. In the first scenario, the laser operator takes the simple form $\hat{V}_{\mathbf{q}_L} = \sum_{\mathbf{p}} m^{\dagger}_{\mathbf{p}+\mathbf{q}_L,f} m_{\mathbf{p},i}$ and, due to the choice of initial state, this results in $\tilde{\beta}_0^{\mathbf{q}_L} = \beta_0^{\mathbf{q}_L} = 1$ and $\tilde{\beta}_{\mathbf{k}}^{\mathbf{q}_L} = 0$. Therefore, $f^{\mathbf{q}_L} = 1$ and the Raman spectrum (B11) reduces exactly to the single particle spectral function.

In the second scenario, the laser operator takes the form $\hat{V}_{\mathbf{q}_L} = \sum_{\mathbf{p}} d^{\dagger}_{\mathbf{p}+\mathbf{q}_L,f} d_{\mathbf{p},i}$. Therefore $\tilde{\beta}_0^{\mathbf{q}_L} = 0$ and, due to our choice of initial state, $\tilde{\beta}_{\mathbf{k}}^{\mathbf{q}_L} = \beta_{\mathbf{k}}^{\mathbf{q}_L}$, which can be simply obtained from minimizing the energy functional $\langle M^{\mathbf{q}_L}|\mathcal{H} - E|M^{\mathbf{q}_L}\rangle$ and is given by

$$|\beta_{\mathbf{k}}^{\mathbf{q}_L}|^2 = \frac{1}{V}\left(\frac{1}{\omega + i0^+ - \varepsilon^c_{\mathbf{k}} - \varepsilon^d_{\mathbf{k}+\mathbf{q}_L} - E_{\mathrm{FS}}(N-1)}\right)^2 \times \frac{1}{\frac{1}{h^2} + \frac{1}{V}\sum_{\mathbf{k}'}\left(\frac{1}{\omega+i0^+-\varepsilon^c_{\mathbf{k}'}-\varepsilon^d_{\mathbf{k}'+\mathbf{q}_L}-E_{\mathrm{FS}}(N-1)}\right)^2}. \tag{B13}$$

APPENDIX C: MOLARON SPECTRAL FUNCTIONS

For illustration see Fig. 5 for molaron spectral functions at several mass imbalances and ranges across the Feshbach resonance, in order to guide experiments.

[1] L. N. Cooper, Bound electron pairs in a degenerate Fermi gas, Phys. Rev. **104**, 1189 (1956).

[2] J. Bardeen, L. N. Cooper, and J. R. Schrieffer, Theory of superconductivity, Phys. Rev. **108**, 1175 (1957).

[3] D. M. Eagles, Possible pairing without superconductivity at low carrier concentrations in bulk and thin-film superconducting semiconductors, Phys. Rev. **186**, 456 (1969).

[4] A. J. Leggett, Diatomic molecules and cooper pairs, in *Modern Trends in the Theory of Condensed Matter*, edited by A. Pękalski and J. A. Przystawa, Lecture Notes in Physics Vol. 115 (Springer, Berlin, 1980).

[5] P. Noziöres and S. Schmitt-Rink, Bose condensation in an attractive fermion gas: From weak to strong coupling superconductivity, J. Low Temp. Phys. **59**, 195 (1985).

[6] C. A. Regal, M. Greiner, and D. S. Jin, Observation of resonance condensation of fermionic atom pairs, Phys. Rev. Lett. **92**, 040403 (2004).

[7] M. W. Zwierlein, C. A. Stan, C. H. Schunck, S. M. F. Raupach, A. J. Kerman, and W. Ketterle, Condensation of pairs of fermionic atoms near a Feshbach resonance, Phys. Rev. Lett. **92**, 120403 (2004).

[8] C. Chin, M. Bartenstein, A. Altmeyer, S. Riedl, S. Jochim, J. H. Denschlag, and R. Grimm, Observation of the pairing gap in a strongly interacting Fermi gas, Science **305**, 1128 (2004).

[9] J. Kinast, S. L. Hemmer, M. E. Gehm, A. Turlapov, and J. E. Thomas, Evidence for superfluidity in a resonantly interacting Fermi gas, Phys. Rev. Lett. **92**, 150402 (2004).

[10] T. Bourdel, L. Khaykovich, J. Cubizolles, J. Zhang, F. Chevy, M. Teichmann, L. Tarruell, S. J. J. M. F. Kokkelmans, and C. Salomon, Experimental study of the BEC-BCS crossover region in lithium 6, Phys. Rev. Lett. **93**, 050401 (2004).

[11] K. E. Strecker, G. B. Partridge, and R. G. Hulet, Conversion of an atomic Fermi gas to a long-lived molecular Bose gas, Phys. Rev. Lett. **91**, 080406 (2003).

[12] J. M. Blatt, K. W. Böer, and W. Brandt, Bose-Einstein condensation of excitons, Phys. Rev. **126**, 1691 (1962).

[13] V. A. Gergel, R. F. Kazarinov, and R. A. Suris, Superfluidity of excitons in semiconductors, Sov. Phys. JETP **27**, 159 (1968).

[14] F. Wilczek, Quantum mechanics of fractional-spin particles, Phys. Rev. Lett. **49**, 957 (1982).

[15] N. Cabibbo and G. Parisi, Exponential hadronic spectrum and quark liberation, Phys. Lett. B **59**, 67 (1975).

[16] F. Scazza, M. Zaccanti, P. Massignan, M. M. Parish, and J. Levinsen, Repulsive Fermi and Bose polarons in quantum gases, Atoms **10**, 55 (2022).

[17] Z. Yan, P. B. Patel, B. Mukherjee, R. J. Fletcher, J. Struck, and M. W. Zwierlein, Boiling a unitary Fermi liquid, Phys. Rev. Lett. **122**, 093401 (2019).

[18] C. J. Vale and M. Zwierlein, Spectroscopic probes of quantum gases, Nat. Phys. **17**, 1305 (2021).

[19] W. E. Liu, Z.-Yu Shi, J. Levinsen, and M. M. Parish, Radio-frequency response and contact of impurities in a quantum gas, Phys. Rev. Lett. **125**, 065301 (2020).

[20] W. E. Liu, Z.-Yu Shi, M. M. Parish, and J. Levinsen, Theory of radio-frequency spectroscopy of impurities in quantum gases, Phys. Rev. A **102**, 023304 (2020).

[21] J. Wang, Multidimensional spectroscopy of heavy impurities in ultracold fermions,Phys. Rev. A **107**, 013305 (2023).

[22] J. Wang, H. Hu, and X.-Ji Liu, Two-dimensional spectroscopic diagnosis of quantum coherence in Fermi polarons, arXiv:2207.14509.

[23] F. Chevy, Universal phase diagram of a strongly interacting Fermi gas with unbalanced spin populations, Phys. Rev. A **74**, 063628 (2006).

[24] N. Prokof'ev and B. Svistunov, Fermi-polaron problem: Diagrammatic Monte Carlo method for divergent sign-alternating series, Phys. Rev. B **77**, 020408(R) (2008).

[25] N. V. Prokof'ev and B. V. Svistunov, Bold diagrammatic Monte Carlo: A generic sign-problem tolerant technique for polaron models and possibly interacting many-body problems, Phys. Rev. B **77**, 125101 (2008).

[26] C. Mora and F. Chevy, Ground state of a tightly bound composite dimer immersed in a Fermi sea, Phys. Rev. A **80**, 033607 (2009).

[27] M. Punk, P. T. Dumitrescu, and W. Zwerger, Polaron-to-molecule transition in a strongly imbalanced Fermi gas, Phys. Rev. A **80**, 053605 (2009).

[28] R. Combescot, S. Giraud, and X. Leyronas, Analytical theory of the dressed bound state in highly polarized Fermi gases, Europhys. Lett. **88**, 60007 (2009).

[29] X. Cui and H. Zhai, Stability of a fully magnetized ferromagnetic state in repulsively interacting ultracold Fermi gases, Phys. Rev. A **81**, 041602(R) (2010).

[30] G. M. Bruun and P. Massignan, Decay of polarons and molecules in a strongly polarized Fermi gas, Phys. Rev. Lett. **105**, 020403 (2010).

[31] R. Schmidt and T. Enss, Excitation spectra and rf response near the polaron-to-molecule transition from the functional renormalization group, Phys. Rev. A **83**, 063620 (2011).

[32] P. Massignan and G. M. Bruun, Repulsive polarons and itinerant ferromagnetism in strongly polarized Fermi gases, Eur. Phys. J. D **65**, 83 (2011).

[33] C. Trefzger and Y. Castin, Impurity in a Fermi sea on a narrow Feshbach resonance: A variational study of the polaronic and dimeronic branches, Phys. Rev. A **85**, 053612 (2012).

[34] C. Kohstall, M. Zaccanti, M. Jag, A. Trenkwalder, P. Massignan, G. M. Bruun, F. Schreck, and R. Grimm, Metastability and coherence of repulsive polarons in a strongly interacting Fermi mixture, Nature (London) **485**, 615 (2012).

[35] A. Schirotzek, Radio-frequency spectroscopy of ultracold atomic Fermi gases, Ph.D. thesis, Massachusetts Institute of Technology, 2010.

[36] M. Alpar and D. Pines, in *The Lives of the Neutron Star: Conference Proceedings*, edited by M. Alpar and J. van Paradijs (Kluwer Academic, Dordrecht, 1995).

[37] M. Sidler, P. Back, O. Cotlet, A. Srivastava, T. Fink, M. Kroner, E. Demler, and A. İmamoğlu, Fermi polaron-polaritons in charge-tunable atomically thin semiconductors, Nat. Phys. **13**, 255 (2017).

[38] A. Schirotzek, C.-H. Wu, A. Sommer, and M. W. Zwierlein, Observation of Fermi polarons in a tunable fermi liquid of ultracold atoms, Phys. Rev. Lett. **102**, 230402 (2009).

[39] G. Ness, C. Shkedrov, Y. Florshaim, O. K. Diessel, J. von Milczewski, R. Schmidt, and Y. Sagi, Observation of a smooth polaron-molecule transition in a degenerate Fermi gas, Phys. Rev. X **10**, 041019 (2020).

[40] P. Fulde and R. A. Ferrell, Superconductivity in a strong spin-exchange field, Phys. Rev. **135**, A550 (1964).

[41] A. I. Larkin and Y. N. Ovchinnikov, Nonuniform state of superconductors, Zh. Eksp. Teor. Fiz. **47**, 1136 (1964).

[42] G. M. Bruun and C. J. Pethick, Effective theory of Feshbach resonances and many-body properties of Fermi gases, Phys. Rev. Lett. **92**, 140404 (2004).

[43] r^* is related to the effective range r_e via $r^* = -r_e/2$.

[44] C. Chin, R. Grimm, P. Julienne, and E. Tiesinga, Feshbach resonances in ultracold gases, Rev. Mod. Phys. **82**, 1225 (2010).

[45] C. J. M. Mathy, M. M. Parish, and D. A. Huse, Trimers, molecules, and polarons in mass-imbalanced atomic Fermi gases, Phys. Rev. Lett. **106**, 166404 (2011).

[46] K. Kamikado, T. Kanazawa, and S. Uchino, Mobile impurity in a Fermi sea from the functional renormalization group analytically continued to real time, Phys. Rev. A **95**, 013612 (2017).

[47] R. Schmidt, T. Enss, V. Pietilä, and E. Demler, Fermi polarons in two dimensions, Phys. Rev. A **85**, 021602(R) (2012).

[48] S. Zöllner, G. M. Bruun, and C. J. Pethick, Polarons and molecules in a two-dimensional Fermi gas, Phys. Rev. A **83**, 021603(R) (2011).

[49] D. E. Sheehy and L. Radzihovsky, Bec-bcs crossover in "magnetized" Feshbach-resonantly paired superfluids, Phys. Rev. Lett. **96**, 060401 (2006).

[50] L. Radzihovsky and D. E. Sheehy, Imbalanced Feshbach-resonant Fermi gases, Rep. Prog. Phys. **73**, 076501 (2010).

[51] N. Yoshida and S.-K. Yip, Larkin-Ovchinnikov state in resonant Fermi gas, Phys. Rev. A **75**, 063601 (2007).

[52] R. Schmidt, M. Knap, D. A. Ivanov, J.-S. You, M. Cetina, and E. Demler, Universal many-body response of heavy impurities coupled to a Fermi sea: a review of recent progress, Rep. Prog. Phys. **81**, 024401 (2018).

[53] H. Hu and X.-J. Liu, Mean-field phase diagrams of imbalanced Fermi gases near a Feshbach resonance, Phys. Rev. A **73**, 051603(R) (2006).

[54] L. He, M. Jin, and P. Zhuang, Loff pairing vs breached pairing in asymmetric fermion superfluids, Phys. Rev. B **73**, 214527 (2006).

[55] Y. He, C.-C. Chien, Q. Chen, and K. Levin, Single-plane-wave Larkin-Ovchinnikov-Fulde-Ferrell state in BCS-BEC crossover, Phys. Rev. A **75**, 021602(R) (2007).

[56] I. Fritsche, C. Baroni, E. Dobler, E. Kirilov, B. Huang, R. Grimm, G. M. Bruun, and P. Massignan, Stability and breakdown of Fermi polarons in a strongly interacting Fermi-Bose mixture, Phys. Rev. A **103**, 053314 (2021).

[57] I. Gotlibovych, T. F. Schmidutz, A. L. Gaunt, N. Navon, R. P. Smith, and Z. Hadzibabic, Observing properties of an interacting homogeneous Bose-Einstein condensate: Heisenberg-limited momentum spread, interaction energy, and free-expansion dynamics, Phys. Rev. A **89**, 061604(R) (2014).

[58] C. Shkedrov, G. Ness, Y. Florshaim, and Y. Sagi, *In situ* momentum-distribution measurement of a quantum degenerate Fermi gas using Raman spectroscopy, Phys. Rev. A **101**, 013609 (2020).

[59] C. Shkedrov, M. Menashes, G. Ness, A. Vainbaum, E. Altman, and Y. Sagi, Absence of heating in a uniform Fermi gas created by periodic driving, Phys. Rev. X **12**, 011041 (2022).

[60] C. Ospelkaus, S. Ospelkaus, L. Humbert, P. Ernst, K. Sengstock, and K. Bongs, Ultracold heteronuclear molecules in a 3D optical lattice, Phys. Rev. Lett. **97**, 120402 (2006).

[61] J. J. Zirbel, K.-K. Ni, S. Ospelkaus, J. P. D'Incao, C. E. Wieman, J. Ye, and D. S. Jin, Collisional stability of fermionic Feshbach molecules, Phys. Rev. Lett. **100**, 143201 (2008).

[62] J. J. Zirbel, K.-K. Ni, S. Ospelkaus, T. L. Nicholson, M. L. Olsen, P. S. Julienne, C. E. Wieman, J. Ye, and D. S. Jin, Heteronuclear molecules in an optical dipole trap, Phys. Rev. A **78**, 013416 (2008).

[63] C. Klempt, T. Henninger, O. Topic, M. Scherer, L. Kattner, E. Tiemann, W. Ertmer, and J. J. Arlt, Radio-frequency association of heteronuclear Feshbach molecules, Phys. Rev. A **78**, 061602(R) (2008).

[64] C.-H. Wu, J. W. Park, P. Ahmadi, S. Will, and M. W. Zwierlein, Ultracold fermionic Feshbach molecules of ^{23}Na^{40}K, Phys. Rev. Lett. **109**, 085301 (2012).

[65] P. S. Julienne and J. M. Hutson, Contrasting the wide Feshbach resonances in ^{6}Li and ^{7}Li, Phys. Rev. A **89**, 052715 (2014).

[66] A. T. Sommer, L. W. Cheuk, M. J. H. Ku, W. S. Bakr, and M. W. Zwierlein, Evolution of fermion pairing from three to two dimensions, Phys. Rev. Lett. **108**, 045302 (2012).

[67] Note that we refer here to an "open channel" as the channel in which particles resides asymptotically in the scattering process. Using this terminology a channel is also closed for a Feshbach molecule when it is below the collision threshold.

[68] It should be noted, however, that for certain observables such a redistribution is important such as when one aims to infer decay rates of quasiparticles from spectral functions.

[69] C. Peng, R. Liu, W. Zhang, and X. Cui, Nature of the polaron-molecule transition in Fermi polarons, Phys. Rev. A **103**, 063312 (2021).

[70] M. M. Parish, H. S. Adlong, W. E. Liu, and J. Levinsen, Thermodynamic signatures of the polaron-molecule transition in a Fermi gas, Phys. Rev. A **103**, 023312 (2021).

[71] X. Cui, Fermi polaron revisited: Polaron-molecule transition and coexistence, Phys. Rev. A **102**, 061301(R) (2020).

[72] R. Liu, C. Peng, and X. Cui, Emergence of crystalline few-body correlations in mass-imbalanced Fermi polarons, Cell Rep. Phys. Sci. **3**, 100993 (2022).

[73] M. E. Gehm, Preparation of an optically-trapped degenerate Fermi gas of ^{6}Li: Finding the route to degeneracy, Ph.D. thesis, Duke University, 2003.

[74] B. R. Johnson, The renormalized Numerov method applied to calculating bound states of the coupled-channel Schroedinger equation, J. Chem. Phys. **69**, 4678 (1978).

[75] J. Vigo-Aguiar and H. Ramos, A variable-step Numerov method for the numerical solution of the Schrödinger equation, J. Math. Chem. **37**, 255 (2005).